1 Introduction

This chapter discusses the importance of detecting drugs and food adulterants at trace levels. It also provides an overview of traditional analytical methods used for trace sensing of these molecules. The chapter delves into the history of Raman spectroscopy and the instruments used to record Raman signals. Additionally, it covers the different modalities of substrate fabrication for Surface-enhanced Raman Spectroscopy that have evolved over time. A brief overview of the machine learning based classification algorithms has also been discussed. Finally, the chapter outlines the motivation of present research study and the research objectives.

1.1 Need for trace sensing of drugs in water and food matrices

The importance of drugs in treating various ailments and maintaining a healthy life cannot be overstated. However, it is crucial to recognize that the improper disposal of pharmaceutical waste could cause significant harm to our natural water resources and aquatic life. The contamination of pharmaceutical waste in natural water resources may lead to the alteration of the abundance of proteins associated with different cell functions of aquatic lives [1]. Amongst the various natural and man-made pollution factors, the household and pharmaceutical waste contribute majorly to the pollution of water bodies. According to the World Health Organization (WHO) report that almost 15% of medical waste is considered hazardous, emphasizing the need for proper disposal methods [2]. Additionally, the presence of antibiotics in different food matrices is a serious concern, as it contributes to antibiotic resistance (AR) and poses a significant threat to human health. According to the Centre for Disease Control, nearly 60,000 children in the USA die before the age of 4 weeks due to antibiotic resistance [3]. In Europe, over 25,000 deaths per year are estimated

which is caused due to various diseases related to AR [4]. Antibiotics are widely used in animal husbandry to treat a range of diseases, with almost 70% of antibiotics produced worldwide being used in poultry. India is among the top five countries with a significant stake in global antimicrobial consumption in animal husbandry [5]. While the prescribed dosage can kill microbial growth in animals, a low dosage of antibiotics can promote muscle growth in animals, leading to increased weight gain [4]. Some of these antibiotics are also used to treat microbial infections in humans [6]. The extensive use of antibiotics in animal husbandry is expected to accelerate the growth of antibiotic resistance in microorganisms, which may cause problems such as treatment failures in human medicine. The following sections then discusses the need for Raman spectroscopy, and the surface-enhanced Raman spectroscopy (SERS) in particular, which has emerged as a unique sensing platform in recent times for detection and analysis of drugs and food adulterants at trace concentrations.

1.2 Traditional sensing modalities

The standard instruments for the detection and analysis of drug samples include liquid chromatography-mass spectrometry, gas chromatography-mass spectrometry, and high-performance liquid chromatography. While these analytical techniques are highly accurate, they often suffer from high cost, long sample preparation times, and are not field portable. These techniques are briefly discussed below-

1.2.1 Liquid chromatography-mass spectrometry

Liquid chromatography-mass spectrometry (LC-MS) is a powerful analytical technique widely used in chemistry and biochemistry for the identification, quantification, and characterization of chemical compounds [7–10]. LC is a separation technique that separates the components in a liquid mixture based on their interaction with a stationary phase and a mobile phase. The sample components are dissolved in a liquid (mobile phase) and pass through a column containing a stationary phase. Different components interact differently with the stationary phase, resulting in their separation. On the other hand, MS is a technique used to identify and quantify molecules based on their mass-to-charge ratio. In MS, ions are generated from sample molecules and then separated based on their mass-to-charge ratio in a magnetic or electric field. The resulting mass spectrum provides information about the composition and structure of the analyzed compounds. LC-MS combines the separation capabilities of liquid chromatography with the sensitivity and specificity of mass spectrometry. After separation by liquid chromatography, the eluent (liquid containing separated components) is introduced into the mass spectrometer for analysis. LC-MS can de-

tect and identify compounds at very low concentrations and is suitable for a broad range of compounds, including small molecules, peptides, and proteins. Furthermore, MS provides information about the molecular weight and structure of compounds. In tandem mass spectrometry, multiple stages of mass spectrometry are performed in sequence, providing additional information about the structure and composition of the analysed compounds [11].

1.2.2 Gas chromatography-mass spectrometry

Gas chromatography-mass spectrometry (GC-MS) is a powerful analytical technique used for the identification and quantification of chemical compounds in a wide range of samples [12–14]. It combines the separation capabilities of gas chromatography with the detection and characterization capabilities of mass spectrometry. GC is a separation technique that separates volatile compounds based on their interaction with a stationary phase and a carrier gas. The sample is injected into the GC system and vaporized. The vaporized sample is then carried through a chromatographic column by a flowing inert gas. Different compounds interact differently with the stationary phase, leading to their separation along the column. MS is a technique used to identify and quantify molecules based on their mass-to-charge ratio. In MS, ions are generated from sample molecules, and these ions are separated based on their mass-to-charge ratio in a magnetic or electric field. The resulting mass spectrum provides information about the molecular weight and structure of the analysed compounds. In GC-MS, the effluent from the gas chromatograph is introduced into the mass spectrometer for analysis. The separated compounds are ionized within the mass spectrometer, and the resulting ions are analysed to produce a mass spectrum. GC provides excellent separation of volatile compounds. MS offers high sensitivity, allowing for the detection of compounds at low concentrations. The combination of GC and MS provides high selectivity for compound identification. Similar to LC-MS, GC-MS can also be configured as a tandem mass spectrometer, allowing for multiple stages of mass spectrometry in sequence for enhanced structural information [15].

1.2.3 High-performance liquid chromatography

High-performance liquid chromatography (HPLC) is a powerful analytical technique used for the separation, identification, and quantification of chemical compounds in a liquid sample [16–19]. HPLC operates on the principles of liquid chromatography, where a liquid mobile phase is used to transport a sample through a stationary phase. The stationary phase, often packed in a column, interacts with sample components based on their chemical properties, leading to separation. HPLC is mainly consist of three major components mobile phase, stationary phase and column. Mobile phase is

a liquid solvent or a mixture of solvents that carries the sample through the column. Stationary phase is a solid or liquid phase that interacts with the sample components, facilitating their separation. Column is a key component where the separation of sample components occurs. The time it takes for a compound to travel through the column and reach the detector is known as the retention time. It is a characteristic property used for identification of various elements present in the analyte. Various detectors are used to monitor and quantify separated compounds, such as UV-Vis detectors, fluorescence detectors, diode array detectors, and mass spectrometers [20, 21]. Detection depends on the specific properties of the compounds being analysed.

1.3 Raman spectroscopy as a sensing technique

Raman spectroscopy is a molecular spectroscopic technique that is known for its high specificity and ability to fingerprint the molecules. It is an inelastic scattering process of light; where almost 1 in $10^6 - 10^8$ photons scatter inelastically. This effect is observed for the first time in India by Sir C.V. Raman and K.S. Krishnan with a rudimentary experimental setup using the sun as the excitation source and his eyes as the detector [22–25]. However, due to low scattering crosssection, the delicate spectroscopic technique was unable to gain much popularity until the 1960s. After the advent of state-of-the-art laser technology the shortcoming of low scattering cross-section has been addressed to a great extent and the applications were explored in different areas like chemical detection, drug detection biomolecule detection [26–28]. Now, there are more than 25 different types of known Raman spectroscopy techniques. To name a few include Stimulated Raman scattering, hyper Raman scattering, Fourier transform Raman scattering, Coherent antistokes Raman Spectroscopy (CARS), and SERS.

1.4 Theory of Raman Spectroscopy

The phenomenon of Raman scattering can be explained theoretically by assuming a classical approach. Classically, light is considered to be an electromagnetic wave that consists of oscillating electric and magnetic fields. Upon irradiating a sample with light, the oscillating electromagnetic field of light distorts the electron cloud, resulting in a change in polarisability [29, 30]. Due to periodic deformation in the electron cloud, the molecules begin to vibrate with its characteristic frequency. If P is polarisability vector and E is the applied electric field of the incident light then

$$P = \alpha E \tag{1.1}$$

For simplicity, we can understand Raman Spectroscopy by assuming a diatomic molecule and approximating the chemical bond between the atoms as a spring, as shown in the figure 1.1,

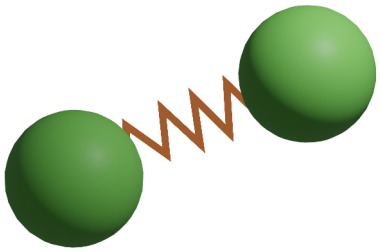

Figure 1.1: Schematic representation of diatomic molecule

Using, Hooke's law of elasticity to the diatomic system, we get

$$\frac{m_1 \times m_2}{m_1 + m_2}\left(\frac{d^2x_1}{dt^2} + \frac{d^2x_2}{dt^2}\right) = -k(x_1 + x_2) \tag{1.2}$$

Denoting the term $\frac{m_1 \times m_2}{m_1 + m_2}\left(\frac{d^2x_1}{dt^2} + \frac{d^2x_2}{dt^2}\right)$ as the reduced mass of the system μ and total displacement $(x_1 + x_2)$ as q, we get

$$\mu\frac{d^2q}{dt^2} = -kq \tag{1.3}$$

Equation 1.3 can be solved by assuming the coordinate variable as follows

$$q = q_0 cos(2\pi\nu_m t) \tag{1.4}$$

where q_0 is the amplitude of the molecular vibration and ν_m is the frequency of the molecular vibration and is defined as,

$$\nu_m = \frac{1}{2\pi}\sqrt{\frac{k}{\mu}} \tag{1.5}$$

The electric field E is given by

$$E = E_0 cos(\omega t) = E_0 cos(2\pi\nu t) \tag{1.6}$$

where E_0 is the amplitude and ν_m is the frequency of the incident electric field. Using equation 1.1 and 1.6, the polarisation of the molecule is given by

$$P = \alpha E_0 cos(2\pi\nu t) \tag{1.7}$$

The oscillating induced dipoles emits radiation at its own oscillating frequency ν which gives rise to Rayleigh scattering. The variation of polarisability with the

molecular vibration gives rises to the inelastically scattered light i.e. the Raman scattered light. This said variation can be written as

$$\alpha = \alpha_0 + q\frac{\partial\alpha}{\partial q} + ... \tag{1.8}$$

Retaining only the first order terms and using equation 1.4 in 1.8 we get

$$\alpha = \alpha_0 + q_0\left(\frac{\partial\alpha}{\partial q}\right)_{q=0} cos(2\pi v_m t) \tag{1.9}$$

Substituting α in equation 1.7, we get

$$\begin{aligned} P &= \left\{\alpha_0 + q_0\left(\frac{\partial\alpha}{\partial q}\right)_{q=0} cos(2\pi v_m t)\right\} E_0 cos(2\pi\nu t) \\ \implies P &= \alpha_0 E_0 cos(2\pi\nu t) + q_0 E_0 cos(2\pi\nu_m t) cos(2\pi\nu t)\left(\frac{\partial\alpha}{\partial q}\right)_{q=0} \end{aligned} \tag{1.10}$$

Using, the trignometric identity $cos(a+b) + cos(a-b) = 2cos(a)cos(b)$ in 1.10 we get

$$\begin{aligned} P &= \alpha_0 E_0 cos(2\pi\nu t) + \frac{1}{2} q_0 E_0\left(\frac{\partial\alpha}{\partial q}\right)_{q=0} [cos(2\pi\nu_m t + 2\pi\nu t) + cos(2\pi\nu_m t - 2\pi\nu t)] \\ \implies P &= \alpha_0 E_0 cos(2\pi\nu t) + \frac{1}{2} q_0 E_0\left(\frac{\partial\alpha}{\partial q}\right)_{q=0} [cos2\pi(\nu_m + \nu)t + cos2\pi(\nu_m - \nu)t)] \end{aligned} \tag{1.11}$$

From equation 1.11 it's evident that the induced electric dipoles have three distinct frequencies viz. the frequency of excitation radiation (ν), the other components ($\nu_m + \nu$) and ($\nu_m - \nu$). During a scattering process, there are two types of frequency components: the dominant one is called Rayleigh scattering, where no change in frequency takes place. The other frequency components account for inelastically scattered radiation, which is referred to as Raman scattering. When there is an up-conversion of frequency, it's known as anti-Stokes radiation, and when there is a down-conversion of frequency component, it's known as Stokes radiation. When a molecule is excited with radiation, the polarizability of the molecule changes, resulting in scattered radiation. However, if the electron cloud of the molecule is not perturbed upon excitation, the net polarizability change is zero, and the scattered radiation will be absent i.e. $\left(\frac{\partial\alpha}{\partial q}\right)_{q=0} = 0$. This means that the radiation will only consist of the incident light. For a molecule to be Raman active, the molecular vibration or rotation must cause a change in the polarizability of the molecule. Sym-

metrical vibrations cause significant changes in the polarizability, resulting in intense Raman scattered signals. On the other hand, asymmetric vibrations result in weak Raman scattered signals, unlike those observed in infrared spectroscopy. In a centrosymmetric molecule, no band can be active in both Raman scattering and infrared absorption. This is referred to as the mutual exclusion rule. The classical approach can explain the emergence of Stokes and anti-Stokes radiation. However, it is unable to explain the different intensities observed in the scattered radiation.

In the quantum mechanical approach, light is viewed as packets of energy known as quanta. When a beam of light falls on a molecule, it interacts with the cloud of electrons surrounding the nuclei [31]. This interaction causes the electrons to polarize and form a short-lived state called the virtual state. The virtual state is not a real state of the molecule but is formed when the laser interacts with the electrons. The energy of the virtual state is determined by the frequency of the light source used. However, this state is not stable and re-radiation occurs quickly. If the process of scattering only distorts the electron cloud, the photons will scatter with small changes in frequency. This type of scattering is called elastic scattering. When molecules scatter light in this way, it is known as Rayleigh scattering. However, if the nuclear motion is induced during the scattering process, energy transfer occurs, and the nature of the process is inelastic scattering. This type of scattering is known as Raman scattering. In Raman scattering, the molecule absorbs energy from the ground vibrational state and is promoted to a higher energy excited vibrational state. This process is called Stokes scattering. However, due to thermal energy, some molecules may exist in an excited state. Scattering from such excited states is known as anti-Stokes scattering and involves transferring energy to the scattered photon. The relative intensities of the two processes depend on the population of the various states of the molecule and are given by the Boltzmann equation (ref figure 1.2) [31].

$$\frac{N_n}{N_m} = \frac{g_n}{g_m} exp\left(-\frac{(E_n - E_m)}{kT}\right) \tag{1.12}$$

where, N_n is the number of molecules in the excited vibrational energy level (n), N_m is the number of molecules in the ground vibrational energy level (m), g is the degeneracy of the levels n and m, E_n-E_m is the difference in energy between the vibrational energy levels and k is Boltzmanns constant. At room temperature, only a small number of molecules are expected to be in an excited vibrational state other than any low-energy ones. As a result, anti-Stokes scattering is weak, especially at higher frequencies. Therefore, Raman scattering is usually recorded only on the Stokes scattering side. However, in some special circumstances, anti-Stokes scattering is preferred. This is done to eliminate the interfering fluorescence noise that occurs at the lower energy side, i.e., on the Stokes scattering side.

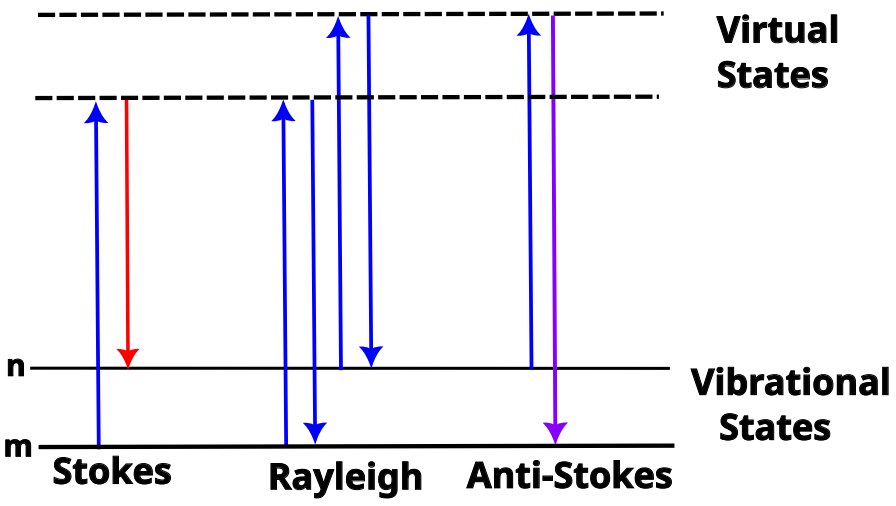

Figure 1.2: Energy diagram of the Rayleigh and Raman scattering processes

The intensites of the scattered Raman bands are illustrated by the equation 1.13

$$I = Kl\alpha^2 w^4 \tag{1.13}$$

where, K is a constant, l is the laser power, α the polarizability of the electrons in the molecule and ω is the frequency of the incident radiation. The parameters l and w are the experimentally controlled parameters and can be tuned for the optimized Raman intensity which has been evident from the equation 1.13.

The Kramer Heisenberg Dirac (KHD) equation [31–34] is used to describe induced polarizability in the molecule and is given by equation 1.14.

$$\alpha_{\rho\sigma} = k\Sigma_l \left(\frac{< F|r_\rho|I >< I|r_\sigma|G >}{\omega_{GI} - \omega_L - i\Gamma_I} + \frac{< I|r_\rho|G >< F|r_\sigma|I >}{\omega_{IF} + \omega_L - i\Gamma_I} \right) \tag{1.14}$$

In the equation 1.14, α denotes the molecular polarisability whereas ρ and σ indicates the directions of incident and scattered polarizations. Σ designates the sum of all vibronic states of the molecule; the remaining constant terms are designated by k. The states $|G>$, $|I>$ and $|F>$ correspond to the ground, excited and final vibrational state respectively. The operators r_σ and r_ρ are the dipole operators. In the term $< I|r_\sigma|G >$ denotes the mixing of two states and is a contributing part in the excitation process. Again, the term $< F|r_\rho|I >$ represents the scattering process and this leaves the molecule in the final state $|F>$. Thus, to conclude, the first two terms in equation 1.14 indicate the mixing of a ground and an excited state and the excited state and the final state respectively. Owing to the mixing nature of the process, the process generally starts in the ground state. Thus, in the second term in

equation 1.14, an equivalent expression has been added to the first term. The added term $< I|r_\rho|G >$ designates the mixing of excited state and the ground state, and $< F|r_\sigma|I >$ represents the mixing of final and the excited state.

When the light is incident on a molecule the virtual state is generated; so it represents the state of the distorted molecule. Since the nuclei do not have time to reach equilibrium, the virtual state is not a state associated with the static molecule. Thus, with the aid of KHD expression the process of distortion is illlustrated by mixing all of the vibronic, excited and ground states together to represent the electronic states of the molecule. In equation 1.14, the energy of the term $i\Gamma_I$ is small when compared to the energies ω_{GI} and ω_L. Additionally, since ω_{GI} and ω_L are added in the second expression, the denominator will always be larger than that in the first term. As a result, term 2 has a smaller impact on describing the polarization process and can be disregarded. If $i\Gamma_I$ was not present, for $\omega_{GI} = \omega_L$ would cause the denominator of the first term to become zero, leading to infinite scattering. The term $i\Gamma_I$ relates to the lifetime of the excited state and influences the natural breadth of Raman lines. By incorporating the Born-Oppenheimer approach in the KHD expression, the selection rules of the scattering process can be determined. The analysis indicates that only vibrations containing one quantum of energy will facilitate Raman scattering, which suggests a good selection rule. Furthermore, it is evident that symmetric vibrations are allowed for Raman scattering. Incorporating the quantum treatment of Raman scattering, it is possible to show that the power of the scattered radiation is proportional to the wavelength and the Raman crossection.

$$\sigma_R \propto \frac{1}{\lambda^4} \tag{1.15}$$

where λ is the wavelength of incident photon and so we get

$$P_s \propto \frac{I_0}{\lambda^4} \tag{1.16}$$

From equation, 1.15 and 1.16, we may conclude that with the short wavelength excitation sources and with the sources with large powers will facilitate Raman spectra with enhanced signal to noise ratio.

1.5 Raman instrumentation

The Raman instrument is composed of four major components: an excitation source, light collection optics, a wavelength selector, and a detector [35–38]. The schematic of a moden Raman instrument is depicted in figure 1.3. In modern Raman spectrometers, a laser is typically used as the excitation source. The collected light is guided to the detector area through light collection optics. Wavelength selectors, which consist

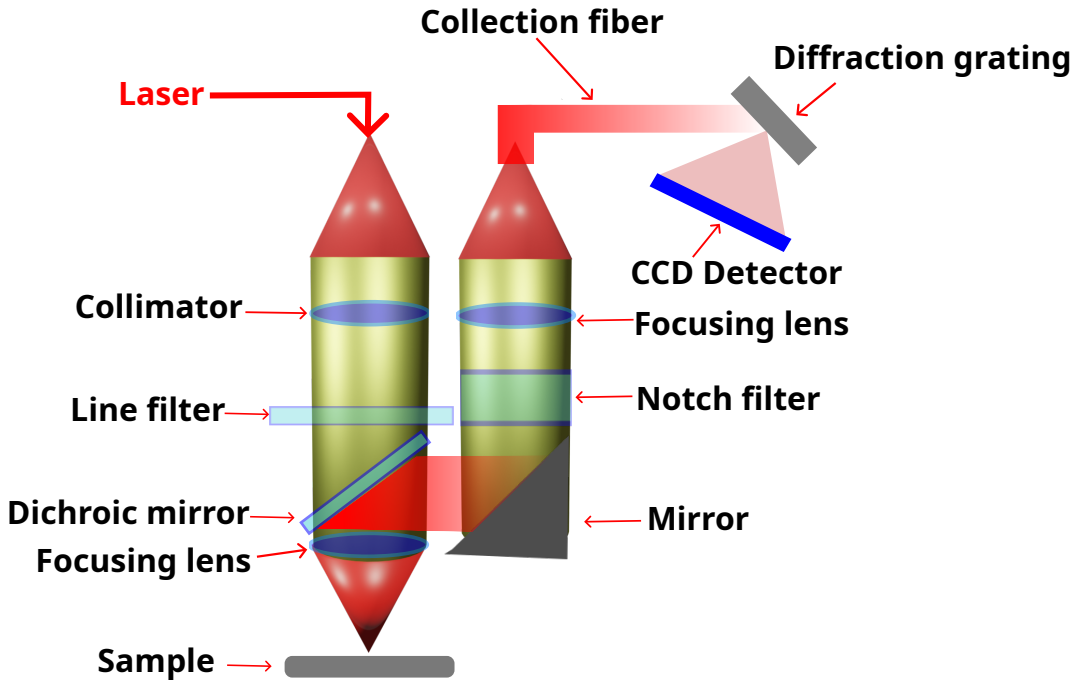

Figure 1.3: Schematic of Raman instrumentation

of monochromators, notch filters, and diffraction gratings, are used to segregate the wavelength-shifted Raman scattering light from the Rayleigh scattered light. The first monochromator is primarily used to separate the frequency-shifted Raman scattering from other radiation. The second monochromator increases the dispersion and separates individual Raman peaks. However, modern spectrometers use notch filters, which absorb all the frequency of incident radiation. With the advancement of modern filters like notch and edge filters, the size of the Raman instrument has been reduced significantly. Most of the commercially available Raman instruments collect scattered light through the notch filter and focus it into a monochromator, which separates the different energies of the Raman bands. The radiation is then directed onto a charge-coupled device (CCD) for detection. In FT-Raman systems, InGaAs detectors are often used for this purpose.

As shown in figure 1.4, there are two basic ways to collect scattered Raman signals: one at 90° while the other at 180° [39]. For 90° scattering method, the laser beam is passed through the sample and the scattered light is then collected at a 90° angle by placing a mirror in a suitable position. The collected light is then imaged onto the entrance slit of the Raman spectrometer. Since the light is scattered as a sphere, it is better to collect a larger cone of light. Therefore, large lense diameter, or lenses with short focal lengths, are used to cover the largest practicable angle. However, it is also necessary to match the collection lenses with the collection optics for efficient

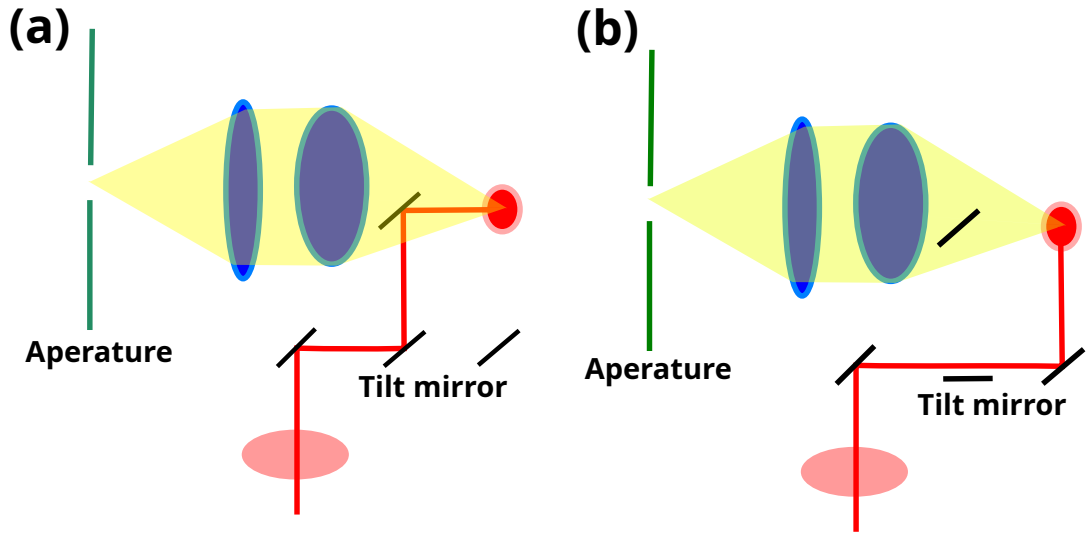

Figure 1.4: Collection optics of Raman (a) at 90° scattering (b) at 180° scattering

performance. In the 180° system, the laser is delivered through the collection lens, and the scattered light is collected back through it. In this arrangement, a small mirror is placed in front of the collection lens to achieve this. This is the common arrangement in systems that use a microscope to collect the light. Sometimes a mirror system such as a Cassegranian system or a silvered sphere is also used, but lenses are more common for Raman instrumentations. In special circumstances, 'grazing incidence' is used, in which the laser beam is directed along the surface.

As has been evident from equation 1.13, the intensity of the scattered Raman signal is related to the power of the laser used for the excitation, the square of the polarisability and the fourth power of the frequency of excitation source. Thus, there are two instrumentation parameters frequency of the source and the laser power which can be tuned to obtain optimized scattered signal from the analyte. Depending on the target application UV, visible and near infrared (NIR) excitation sources are being employed to record the scattered Raman signals. Often in many spectrometers UV excitation is preferred, due to the fact that the scattered intensity varying with the fourth power of the frequency (ref to equation 1.13), which also ensures enhanced Raman sensitivity. Also, occurrence of fluorescence is less probable in the UV excitation region as compared to the visible excitation. However, UV excitation suffers from some serious drawbacks such as sample heating and sample degradation may occur; as many samples absorb UV radiation. Additionally, quality of optics required for the UV excitation sources is different from visible sources; the cost associated with it are quite high. So, visible excitation sources are often preferred as they are readily available and can be quite compact. The primary and most significant drawback of using visible excitation is fluorescence, which is present in all visible Raman spectrometer systems. More often, high power densities are used due to the lack of

sensitivity in the visible excitation; which makes the fluorescene more feasible in that range. Again, in most of the cases or in industrial use to be able to record the Raman spectra for most of the samples NIR laser are preferred; which is often equipped with an interferometer. The main advantage of the NIR based excitation system is that fluorescene is less probable in that range; since most of the molcules don't have excitation wavelength in NIR range. Generally, a neodymium-doped yttrium aluminium garnet (Nd^{3+}:YAG) solid state laser emitting at 1064 nm is used. Since the excitation wavelength is much longer (weaker radiation) most of the samples donot absorb the exciting radiation efficiently compared to the visible and UV region; for this reason high laser powers ($\sim$2 watts) are used with these configurations. The coupling of the FT-based system makes the spectrometer very sensitive. At room temperatures, the detectors normally used are InGaAs based detectors, however for enhanced sensitivity the detector can be cooled to liquid nitrogen temperatures. Further, the microscope can be attached with NIR based system, however thermal degradation may result owing to the high power density at the focal point. Generally, in the NIR based systems occurrence of fluorescence could be avoided to a large extent.

Modern visible spectrometer are extended by using NIR lasers as the excitation source with wavelengths in the range 785-850 nm. These systems can be used to analyse a wide variety of samples for which Raman scattering can be measured effectively without fluorescence interference. In these instruments, CCD is used as the detector which are inaffective at the wavelengths above 1000 nm. The major problem for the manufacturers of visible source instruments is that the CCD chips lack sensitivity at wavelengths above 1000 nm. This means that lasers that operate at 790 nm or 850 nm are effective but are also very close to the end of the detector range which eventually would lead to a drop in sensitivity for higher wavelength peaks.

1.6 Limitations of Raman Spectroscopy

Raman scattering is a very weak process, almost 1 in 10^7 photons scatters inelastically contributing to low scattering cross-section ($\sim 10^{-30}$ cm^{-2}) of Raman spectra. The wide applications of the technique in different domains were limited due to low-sensitivity; compared to the other spectroscopic techniques such as fluorescence spectroscopy. However, the invention of laser in 1960s makes it possible for utilizing the technique in different domains of chemical and biomolecule detection. Even after the incorporation of laser as the excitation source the technique is not capable of detecting low concentration samples. SERS emerges as a good alternative in the realm of near-field Raman where the low-sensitivity issue could be greatly addressed to a good extent [40–43]. Owing to the effect of strong LSPR in the metal nanostructure, the intensities of the scattered Raman signals from the target analyte are enhanced

manifold once it is brought to the vicinities of the metal nanoparticles.

1.7 Surface-enhanced Raman Scattering

The phenomenon of SERS was first observed in 1974 by Fleischman et al [44]. They reported strong Raman scattering from pyridine molecules adsorbed from an aqueous solution onto a silver electrode, which was roughened using successive oxidation-reduction cycles. Initially, the effect was attributed to an increase in the electrode surface area caused by the roughening process, which enabled more pyridine molecules to be absorbed on the surface. However, two independent groups showed that the enhancement was not caused by the roughening of the electrode, as roughening could only contribute to a 10-fold enhancement in the Raman bands, whereas the observed signal enhancement was of the order of 10^6 [45, 46]. Moskovits established that the contribution of optical properties in metallic surfaces was the cause of the enhancement [47]. This new optical phenomenon leads to the naming of the method as SERS. It became evident that roughened Ag electrodes were not the only type of material that can be used as SERS substrates. Pettinger, Wenning, and Wetzel demonstrated the use of Au, Ag, and Cu electrodes for the enhancement in Raman signals pyridine. The optical properties of metals like Ag, Au, and Cu suggest resonances in the visible region, supported by the surface plasmons (SPs). [47, 48]. The surface enhancement is caused by SPs' excitation, which triggers the enhancement in the electric field localized near the metallic nanostructures. If the nanostructures are very near, about 1-2 nm, the local electric field is enhanced by a substantial value. These regions are known as SERS hotspots [49]. The electromagnetic component described by the Surface Plasmon successfully explained the experimental results to a great extent. However, in some cases, it failed to explain the chemical contribution. The optical model does not consider the enhancement's dependence on the chemical factors of the probe molecule.

1.8 Theory of SERS

The true nature of the theory of SERS is still an active field of research; however two contributing mechanisms - electromagnetic (EM) enhancement [50] and the chemical enhancement [51] are assumed to be the primary cause from which most of the observed results can be correctly explained. When an analyte is adsorbed onto metal surface or resides in the close proximity to the metal surface; an interaction occurs between the analyte and the plasmons. This interaction is known as electromagnetic enhancement and is the primary contributor in scattered Raman signal enhancement process. Again, when the adsorbate molecule chemically bonds to the surface, excita-

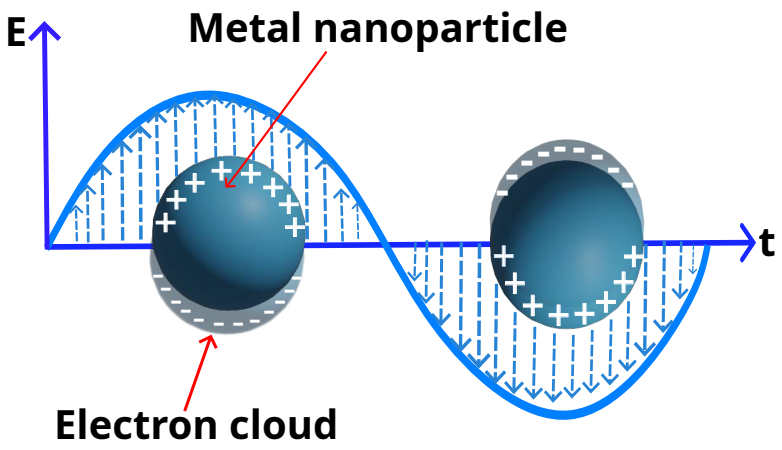

Figure 1.5: Localised surface plasmon resonance

tion is then through transfer of electrons from the metal to the molecule and back to the metal again. This form of enhancement is known as charge transfer or chemical enhancement; this contributes only $\sim 10^3$ in the enhancement process.

1.8.1 EM enhancement

Metal surfaces like silver have ample amount of electrons contributed from the conduction band. When a metal is irradiated with light, a collective group of oscillations results across the metal surface; these oscillations are termed as surface plasmons. Figure 1.5 shows the schematic representation of surface plasmon on metal dielectric interface. Surface plasmons resulting from uniform metal nanostructures, or from metal surfaces having a single periodic roughness, have a resonance frequency at which the absorption and scattering occur most efficiently. The resonance frequency varies with the metal and the nature of the surface. The oscillation frequency for silver and gold lies in the visible region; so these metals are useful in visible region and NIR based excitation sources. For smooth surface the oscillation occurs along the plane of the surface resulting in absorption but no scattering. To get scattering, there needs to be an oscillation perpendicular to the surface and this is achieved by roughening the metal surface. Another important parameter of interest is the ratio of absorption to scattering. The real part of the dielectric constant of a material designates the scattering process, whereas the imaginary part designates the absorption part of a material. Silver is reported to be have comparatively good scattering capability.

The process of EM enhancement can be understood by assuming a small metallic sphere [31] ; however the contribution arising from the roughness of a material is neglected. Let's assume a small metal sphere which is subjected to an applied electric field from the laser, the field at the surface is described by

$$E_r = E_0 cos\theta + g\frac{a^3}{r^3}E_0 cos\theta \tag{1.17}$$

where E_r is the total electric field at a distance r from the sphere surface, a is the radius of the sphere, θ is the angle relative to the direction of the electric field, g is a constant related to the dielectric constants such that

$$g = \frac{\epsilon_1(\nu_L) - \epsilon_0}{\epsilon_1(\nu_L) + 2\epsilon_0} \tag{1.18}$$

ϵ_0 and ϵ_1 are the dielectric constants of the medium surrounding the sphere and of the metal sphere respectively. ν_L is the frequency of the incident radiation. When the denominator of equation 1.18 is at a minimum, the value of g will be maximum when $\epsilon_0 \approx 1$ and consequently this maximum usually occurs when $\epsilon_1 \approx 2$. At this plasmon resonance frequency the excitation of the surface plasmon greatly increases the local field experienced by the molecule absorbed on the metal surface. In brief, the molecule is surrounded in a very freely moving electron cloud and it intensifies the polarization of the surface electrons. The electrons in the analyte molecule adsorbed on the surface interact with this cloud causing greater polarization around the molecule; which results in the enhanced Raman bands of the molecules.

The electromagnetic contribution of the SERS signal could be further assumed to be composed two main enhancements - local field enhancement and radiation enhancement.

Local field enhancement:

The electromagnetic field surrounding metallic surfaces undergoes significant alteration when electromagnetic radiation interacts with a suitable metal surface, characterized by a negative real and small positive imaginary dielectric constant [52]. This condition is feasible when the excitation wavelength λ_L is close to the electromagnetic resonances of the system. This specific alteration in the electromagnetic field arises from the coherent oscillation of free electrons, which give rise to surface plasmons. This results in the generation of EM hotspots and very high local fields contributing to the local field enhancement. The local electric field (E_{Loc}) differs from the incident field (E_{inc}) both in terms of magnitude and orientation. Generally, the magnitude of $|E_{Loc}|$ can be significantly greater than $|E_{inc}|$. The local field induces a Raman dipole moment, given by :

$$P_R = \alpha_R E_{Loc}(\omega_L) \tag{1.19}$$

Thus, the dipole moment is amplified by a factor of $|E_{Loc}(\omega_L)|/|E_{inc}|$ compared to the dipole induced by the incident field. If such a dipole radiates in free space (i.e.,

in the absence of a metallic environment), the radiated energy, which is proportional to $|P_R|^2$, would be enhanced by a factor:

$$M_{Loc}(\omega_L) = \frac{|E_{Loc}(\omega_L)|^2}{|E_{inc}|^2} \tag{1.20}$$

The factor $M_{Loc}(\omega_L)$ is designated as the local field intensity enhancement factor and is associated with the excitation of the Raman dipole. It also characterizes the enhancement of the electric field intensity. Here, any modification of the electric field polarization occurred during the process is neglected.

Radiation enhancement:

In the context of SERS conditions, the dipole moment generated by the local field radiates very near to the metal, and the metal significantly influences this dipole radiation [52] . Depending on factors such as the relative dielectric function $\epsilon(r)$ of the metal, its geometry, the position and orientation of the dipole, and its emission frequency (ω_R), the value of$M^d_{Rad}(\omega_R)$ can either increase or decrease compared to that in free space. The coupling of LSPR in metallic objects results in an enhancement of the radiated power. Therefore, the radiation enhancement factor is given by-

$$M_{rad} = \frac{P_{rad}}{P_0} \tag{1.21}$$

where P_{rad} and P_0 is the total power radiated by the dipole in presence of a medium and the free space respectively. The overall SERS intensity depends on both the incoming (ω_{inc}) and the outgoing ($\omega_s = \omega_{inc} - \omega_{vib}$) field and is given by the equation

$$I_{SERS} = I_{inc}(\omega_{inc}).I(\omega_s) = |E_{inc}(\omega_{inc})|^2|E(\omega_s)|^2 \tag{1.22}$$

For the best SERS enhancement, it's important that the incident radiation at ω_L and the stokes shifted radiation at ω_s are both resonant with the LSPR peak of the metallic nanostructure. Generally, nanostructures with dimensions $\sim$ 30-100 nm are needed for excitation with visible radiation. Additionally, the LSPR is heavily influenced by the size and shape of the nanostructures, and is also strongly altered when nanostructures are closely spaced due to the existence of coupling, which mainly results from the interactions of the LSPR of individual nanostructures. For simple cases, I_{SERS} can be reduced to $|E(\omega_L)|^4$ which is known as E^4 enhancement.

1.8.2 Chemical enhancement

In the context of chemical enhancement (CE), a bond is established between the surface of the metal and the analyte, enabling the transfer of charge from the metal surface into the analyte [51, 53–55]. The formation of this bond results in an increased interaction with the metal electrons, leading to an enhanced molecular polarisability. This enhancement is believed to occur as a result of the emergence of new electronic states that arise from the bond between the analyte and the metal surface. These new states are thought to be resonant intermediates in the Raman scattering process. Unlike the EM enhancement mechanism, the radiation is absorbed into the metal, and a hole is transferred into the adsorbate metal atom cluster. After the Raman process, excitation is transferred back into the metal and re-radiation occurs from the metal surface. Since the CE occurs mostly only from molecules that are directly attached to the surface, it should increase only up to monolayer coverage.

1.8.3 Enhancement Factor

The enhancement factor (EF) stands as a pivotal aspect of the SERS phenomenon. Over time, various types of SERS EFs have been proposed to establish an optimal metric for comparing experiments across diverse substrates and conditions, alongside facilitating theoretical calculations. A standard definition of EF chooses the integral intensities of the strongest band in SERS (I_{SERS}) against those in conventional Non-Resonant Raman Scattering or Resonant Raman Scattering (N_{RS}) spectra. This comparison, normalized to the number of molecular scatterers involved in each scenario and conducted under identical experimental setups, yields

$$EF = \frac{I_{SERS}/N_{SERS}}{I_{RS}/N_{RS}} \tag{1.23}$$

In scenarios like backscattering experiments (e.g., Raman microscopy), the ratio N_{SERS}/N_{RS} is often estimated as the quotient of the effective surface density of adsorbed molecules during SERS measurement to the spatial molecular density in conventional Raman measurements, multiplied by the effective height of the scattered volume [56].

The analytical enhancement factor (AEF), used in SERS analytical applications, considers ratio of molecular concentrations of measured analyte.

$$AEF = \frac{I_{SERS}/c_{SERS}}{I_{RS}/c_{RS}} \tag{1.24}$$

This parameter effectively showcases how surface enhancement facilitates the analytical capability of Raman spectroscopy in specific instances. However, it's notewor-

thy that AEF is not solely contingent on the SERS phenomenon but is also influenced by the substrate type and its coverage by the adsorbate.

1.9 Role of SERS substrate

In the field of SERS, the plasmonic nanostructured platform is commonly referred to as SERS substrates, while the target analytes are called SERS probes. These substrates are crucial in SERS-based sensing and consist primarily of plasmonic nanostructures that support LSPR. The nanoscale roughness and periodicity are essential for achieving a enhanced and reproducible SERS signal. Over the years, different types of SERS substrates have been developed, ranging from electrochemically roughened SERS substrates to lithographically prepared SERS substrates [57]. The selection of substrates is critical in SERS because the interaction between the probe and the substrate is necessary.

1.10 SERS Substrate fabrication

The fabrication of SERS substrates involves a broad spectrum techniques. Some of the methods which are employed in the present thesis work are briefly discussed below

1.10.1 Chemical Synthesis of Nanoparticles

Nanoparticles made of noble metals like gold, silver, or copper are usually synthesized by the chemical reduction method and deposited onto a substrate. The commonly used Lee-Meisel and Turkevish method for synthesizing silver nanoparticles (AgNPs) and gold nanoparticles(AuNPs) fall in this category [58]. These methods require metal precursors, reducing agents, and stabilizing agents. The metal contributes metal ions which are responsible for the formation of metal nanoparticles while the stabilizing agent helps to control the size and stability of the formed nanoparticles. The reducing agent reduces metallic ions to metal nanoparticles by donating electrons. The size and shape of the nanoparticles depend on the rate of addition of the reducing agent and the concentrations of the reactants. The stabilizing agent helps to stabilize the formed nanoparticles and prevent them from agglomerating or precipitating. After the completion of the reaction, the resulting solution is washed or centrifuged to remove any excess reagents and byproducts.

1.10.2 Electrochemical Deposition

Electrochemical deposition is a highly versatile technique that allows for the controlled growth of metal nanostructures on conductive surfaces. This technique is

commonly used for the fabrication of SERS substrates, which are used to enhance Raman signals. The process involves the reduction of metal ions from a solution onto a conducting substrate. To carry out electrochemical deposition, we need a conductive substrate made of materials like indium tin oxide (ITO), gold, or platinum, and a solution containing the metal precursor, typically a salt of the metal to be deposited (e.g. silver nitrate, gold chloride). The concentration of the metal salt and the supporting electrolyte can be adjusted based on the desired properties of the SERS substrate [59–64]. To initiate the reaction that triggers the reduction of metal ions onto the substrate, an electrochemical setup is designed. This setup includes the conductive substrate as the working electrode, a counter electrode (usually platinum), and a reference electrode. By applying a suitable potential to the working electrode (substrate) in the presence of the metal precursor solution, metal ions are reduced onto the substrate, leading to the formation of metal nanostructures. The morphology of the nanostructures can be controlled by adjusting the deposition parameters, which include the applied potential, deposition time, and temperature. To further enhance the SERS activity, some surface modification steps like annealing could be performed.

1.10.3 Electrospinning technique

Electrospinning (ES) is a technique used in the fabrication of SERS substrate for producing polymer nanofibers with diameters ranging from few nanometres to several micrometres. In the ES system, a high voltage is applied to a polymer solution which causes a charged jet of the polymer solution to be released from a syringe needle towards ground collector. During the course of travelling the charged jet stretches and solidifies into ultrafine fibers, which further accumulate on the collector to form a nano mat containing micro and nano-porous structures. Due to the formation of nano-porosity, tunable morphology and high surface area to volume ratio, the electrospun nanofibers facilitates excellent SERS characteristics [65]. The nanofiber based platforms enhances the scattered Raman signals of the analytes adsorbed onto their surfaces, thereby facilitating detection and analysis of analyte molecules at trace concentrations.

The conventional mode of substrate fabrication via ES suffers from issues like non-uniformity and the production of chemical intermediates in the synthesis procedures. By adopting plasma treatment for the generation of NPs, such problems can be resolved to a great extent. In the plasma treatment techniques, the NPs are produced from the metal salts by the process of photo reduction. Thus, the fabrication process is green and thereby doesn't produce any interfering intermediates. Also, plasma treatment parameters can be adjusted to tailor the properties of nanofiber substrates

in accordance to the target applications. For the optimized SERS characteristics the properties such as surface roughness, porosity, and wettability can be tuned by optimizing the plasma etching time and voltages.

1.11 Other techniques

Some other substrate fabrication modalities like Physical Vapor Deposition, Chemical Vapor Deposition, lithography are also rich in SERS literatures and are widely used in commercial SERS substrates. With these techniques very sensitive and reproducible SERS substrates can be fabricated. However, due to the high cost of instrumentation and long fabrication time, such techniques are not suitable for infield sensing purposes. Some of these techniques are briefly discussed below-

Physical Vapor Deposition:

Physical Vapor Deposition (PVD) is a technique used to fabricate SERS substrates [66, 67]. PVD involves depositing material in a physical vapor state onto a substrate surface, creating thin films or nanostructures that enhance Raman signals. Thin films of noble metal nanostructures are deposited using evaporation or sputtering.

Chemical Vapor Deposition:

Chemical Vapor Deposition (CVD) is a technique used for the synthesis of thin films, nanostructures, or coatings by introducing chemical precursors in the vapor phase onto a substrate surface [68, 69]. In the context of SERS, CVD can be employed to design nanostructured surfaces that enhance Raman signals. In this process, the metal precursor is deposited on the substrate surface leading to the formation of nanostructures via thermal activation. The morphology, size, density and distribution of the nanostructures can be tuned by controlling the parameters such as precursor flow rate, temperature, and pressure.

Lithography:

Lithography is a technique used for printing or patterning on a substrate, and it has various applications in microelectronics, nanotechnology, and the production of optical components [70–72]. The principle of lithography involves transferring a pattern from a mask or template onto a substrate. There are various types of lithography techniques available, but the most commonly used are photolithography, electron beam lithography, and nanoimprint lithography. In photolithography, light is used to transfer a pattern from a photomask to a light-sensitive photoresist on a substrate. On the other hand, E-beam lithography uses a focused beam of electrons to directly

write patterns on a substrate and nanoimprint lithography involves pressing a mold into a soft resist layer on a substrate to create a pattern.

1.12 Chemometrics and ML implementation

Chemometrics is the application of statistical and mathematical methods to analyze chemical data [73–75]. It is particularly useful for handling complex datasets generated from analytical techniques such as spectroscopy. In the context of spectroscopy, chemometrics helps extract meaningful information, reduce noise, and make predictions or classifications. Common chemometric techniques include principal component analysis, partial least squares regression (PLS), and cluster analysis. On the other hand, machine learning (ML) is a broader field that involves the development of algorithms and models that enable computers to learn patterns from data without explicit programming [76–79]. In the context of chemical analysis, ML is applied to process and interpret complex datasets. Supervised learning, unsupervised learning, and reinforcement learning are common types. ML models can be trained to recognize patterns, make predictions, classify data, and identify relationships between variables. When applied together, chemometrics and ML enhance the capabilities of chemical analysis techniques. Chemometrics helps preprocess and extract relevant information from data, while ML models can learn complex patterns and relationships within the dataset. This combination is powerful for tasks such as quantitative analysis, pattern recognition, feature selection, and real-time monitoring in various scientific and industrial applications. Chemometrics and ML are related fields that share some common goals, such as extracting information and patterns from complex data sets. However, there are small differences between these two approaches. In Chemometrics, we primarily focus on statistical methods and mathematical modeling for the analysis of chemical data. It is often applied in chemistry, spectroscopy, and analytical chemistry for tasks like calibration, quality control, and pattern recognition. However, ML encompasses a wide range of algorithms and techniques designed to enable computers to learn from data and make predictions or decisions. It has applications in various fields, including computer vision, natural language processing, and healthcare, in addition to chemistry and analytical sciences. The selected chemometrics, ML, and deep learning algorithms implemented in the current thesis work are discussed briefly.

1.12.1 Principal Component Analysis

Principal component analysis (PCA) is a statistical method used for reducing the number of dimensions in a dataset while retaining the most significant informa-

tion and transforming high-dimensional data into a lower-dimensional representation [80, 81]. PCA has two objectives: dimensionality reduction and decorrelation. It aims to transform the data into a set of linearly uncorrelated variables called principal components while preserving the essential variance in the data. These principal components are obtained by linearly combining the original features. The first principal component accounts for the most variance, the second for the second most, and so on. PCA involves finding the eigenvalues and eigenvectors of the covariance matrix of the original data. The eigenvectors define the directions (principal components), and the eigenvalues indicate the amount of variance along those directions. The steps involved in PCA are standardization, estimation of the covariance matrix, eigenvalue decomposition, and selection of principal components. To begin with, PCA calculates the covariance matrix of the original data, which represents the relationships between pairs of features. The covariance matrix is then decomposed into its eigenvectors and eigenvalues. The eigenvectors form the new basis for the data, and the eigenvalues indicate the variance along each corresponding eigenvector. In summary, PCA is a useful technique for dimensionality reduction and data visualization. It aims to transform high-dimensional data into a lower-dimensional representation while retaining the most significant information and decorrelating the features. PCA involves finding the eigenvalues and eigenvectors of the covariance matrix of the original data and selecting the principal components that explain the most variance in the data.

1.12.2 K-Nearest Neighbour algorithm

K-Nearest Neighbors (KNN) is a simple and widely used algorithm for classification and regression tasks in ML [82–84]. It's a type of instance-based learning, where the algorithm makes predictions based on the majority class or average value of its k nearest neighbors in the feature space. KNN involves storing all training examples, prediction for a new data point, calculation of its distance to all other data points in the training set. Further, selection is made for the k-nearest neighbors with the smallest distances to the new data point. In the final step, the majority voting is performed and subsequent the class labels are assigned.

1.12.3 Support Vector Machine and Kernel-Support Vector Machine algorithm

A Support Vector Machine (SVM) is a supervised ML algorithm that is used for classification and regression tasks [85–87]. SVMs are particularly effective in high-dimensional spaces and are well-suited for scenarios where the data points are not easily separable by a linear boundary. For classification problems, SVM aims to find a hyperplane that best separates the data into classes, maximizing the margin between

the classes whereas for regression problems, SVM seeks to find a hyperplane that best fits the data, while allowing for a margin of error. The SVM algorithm finds the hyperplane that maximizes the margin between the classes. The margin is the distance between the hyperplane and the nearest data point from either class. SVM seeks to maximize this margin. The larger the margin, the more robust the classifier is to variations in the data. Support vectors are the data points that lie closest to the decision boundary (hyperplane) and have the most influence on determining the optimal hyperplane. These are the critical elements in SVM that define the margin and the decision boundary. SVM can handle non-linear relationships between features through the use of a kernel function. Common kernel functions include linear, polynomial, radial basis function (RBF), and sigmoid [88]. The choice of kernel depends on the nature of the data. This is known as kernel SVM (KSVM).

1.12.4 Decission tree algorithm

Decision Tree is a ML algorithms used for both classification and regression tasks [89, 90]. Decision Trees are a type of supervised learning algorithm that makes decisions based on a series of conditions. The algorithm builds a tree structure where each internal node represents a decision based on a feature, each branch represents the outcome of the decision, and each leaf node represents the final decision or prediction. In the training step, the tree is built recursively by selecting the best feature to split the data at each node. The selection is based on criteria like Gini impurity (for classification) or mean squared error (for regression). However, decision Trees can be prone to overfitting, capturing noise in the training data and resulting in poor generalization to new data and sensitive to small variations in the data.

1.12.5 Naive Bayes algoritm

The Naive Bayes algorithm is a probabilistic ML algorithm based on Bayes' theorem. Despite its simplicity, it is often quite effective for classification tasks, particularly in natural language processing and text classification [91, 92]. Naive Bayes is built upon Bayes' theorem, which relates the conditional and marginal probabilities of random events. In the context of classification, it helps estimate the probability of a particular class given the observed features [93]. The algorithm assumes that the features used to describe an instance are conditionally independent given the class label.

$$P(class|feature) = \frac{P(feature|class)P(class)}{P(feature)} \tag{1.25}$$

Naive Bayes calculates the probability of each class given the observed features. For a given class, the probability is calculated as the product of the probabilities of

each feature given the class.

$$P(class|feature) \propto P(class)\Pi_{i=1}^{n} P(feature|class) \tag{1.26}$$

During training, the algorithm estimates the prior probability of each class $P(class)$ and the conditional probabilities of each feature given each class $P(feature|class)$. During the classification phase, the algorithm calculates the probability of each class for a given set of features and selects the class with the highest probability as the predicted class.

1.12.6 Aritificial Neural Network

Artificial Neural Network (ANN) is one of the class of ML algorithms inspired by the structure and functioning of the human brain. They consist of interconnected nodes (neurons) organized into layers, each layer having a specific role in the network. ANNs are widely used for various tasks, including classification, regression, pattern recognition, and more [91, 94–96]. Neurons are the basic units in an ANN, and they receive inputs, perform a computation, and produce an output. Neurons are organized into layers, including an input layer, one or more hidden layers, and an output layer. Input Layer receives input features and passes them to the hidden layers. The hidden layers are intermediate layers between the input and output layers where computations are performed. Deep neural networks have multiple hidden layers. The output layer produces the final output of the network. Each connection between neurons has an associated weight, which determines the strength of the connection. Biases are additional parameters that allow the model to learn an offset. Activation functions introduce non-linearities to the model, enabling it to learn complex patterns. Common activation functions include sigmoid, hyperbolic tangent (tanh), and rectified linear unit (ReLU). By the process of feed forward propagation, input is passed through the network to produce an output. Each layer's neurons process the inputs using the weights and biases. The training process involves adjusting the weights and biases based on the difference between the predicted output and the actual target. Backpropagation is an optimization algorithm that iteratively adjusts the network parameters to minimize the error. The lost function measures the difference between the predicted output and the actual target. Common loss functions include mean squared error for regression and cross-entropy for classification. Further, optimization algorithms such as gradient descent and its variants are used to minimize the loss function and update the weights during training. A hyperparameter that determines the step size during weight updates. It influences the convergence and stability of the training process. The number of training examples used in one iteration of gradient descent is called batch size. Epoch denotes the one pass through

the entire training dataset during training process; however multiple epochs may be required to train the network effectively. By hyperparamter tuning it's feasible to adjust parameters like the learning rate, number of hidden layers, and neurons per layer to optimize performance.

1.12.7 Performance evalutation of the ML algoritm

Evaluating the performance of a ML algorithm is crucial to understanding how well it generalizes to new, unseen data. There are several metrics and techniques for performance evaluation, and the choice depends on the type of task (classification, regression, clustering) and the specific goals of your model. Some of the commonly used metrices in classification problems are illustrated below [97, 98]. If TP, TN, FP and FN represents true positive, true negatives, false positives and false negative respectively then

$$Accuracy = \frac{TP + TN}{TP + TN + FP + FN} \tag{1.27}$$

$$Precision = \frac{TP}{TP + FP} \tag{1.28}$$

$$Recall = \frac{TP}{TP + FN} \tag{1.29}$$

$$F1 - score = 2 \times \frac{Precision \times Recall}{Precision + Recall} \tag{1.30}$$

Another important metric which is readily used is area under the receiver operating characteristic (ROC-AUC). It measures the area under the ROC curve, which plots the true positive rate against the false positive rate. Again confusion matrix is another parameter which provides a detailed breakdown of true positives, true negatives, false positives, and false negatives.

1.13 Scope of the thesis and statement of the thesis problem

SERS has emerged as a sensitive analytical technique for reliable detection of analyte molecules in trace concentrations. The choice of SERS substrate is crucial in the sensing process and is specific to the analyte of interest. Obtaining good reproducibility and uniformity characteristics is highly desirable for deploying SERS substrates in the different domains of applications. In addition, the feasibility of a substrate depends on the factors like fabrication time and cost. Thus fabricating SERS substrate involves controlling specific parameters to optimize signal enhancement. The choice

of substrate material plays a crucial role in enhancing Raman signals; common materials include gold, silver, and copper, known for their strong plasmonic properties. Many of the studies reported so far fall short of fulfilling all the requirements for enhanced SERS characteristics. For example, SERS substrates obtained through the electrochemical roughening of electrodes may be cost-effective but often suffer from poor EF and reproducibility issues. On the other hand, colloidal nanostructures can generate high EF but often exhibit low reproducibility. Although lithographic techniques can be employed to fabricate highly reproducible SERS substrates, they require professional training for sample preparation and equipment operation. These techniques involve expensive and sophisticated instruments, as well as the need for a well-equipped laboratory facility. In addition to that the high costs associated with these substrates limit their accessibility.

The present thesis work explores different low-cost modalities of SERS substrate fabrication. The developed SERS substrates has been applied to detect and quantify trace concentrations of drugs in water and various food matrices.

1. At first, a relatively simple yet low-cost SERS platform has been fabricated using 100 GSM paper. In presence of metallic NPs, the micropores of 100 GSM paper facilitates generation of EM hotspot regions in the proposed paper platform. Owing to the phenomena of LSPR in the generated EM hotspots, the scattered Raman signal are enhanced manifold supporting the sensing and quantification of analyte in trace concentrations. Again, with the optimized rate of in-plane diffusion over the lateral diffusion in 100 GSM paper facilitates relatively uniform SERS signal compared to other grade papers. Also, aggregation rate of NPs is found to be optimized in case of the proposed 100 GSM SERS platform, which further supports uniform Raman signals over the sensing region of the SERS substrate. Furthermore, the fabricated SERS platform has been used for detecting trace concentrations of pharmaceutical drugs paracetamol and aspirin in real water samples.

2. In the next work, the natural leaf surfaces have explored for the plausible application as a SERS substrate. Although different groups have explored the leaf surfaces, but the main goal remains confined to fabricate a hydrophobic SERS substrate. The hydrophobic SERS substrates provides extensively strong Raman signals due to the aggregation of nanoparticles in a relatively small area, but these substrate lacks uniformity. To address this issue, a aegle marmelos *(AM)* leaf surface having hydrophilic nature was chosen. The *AM* leaf surface have imprinted micro structured pattern which supports the formation of EM hotspots regions when deposited with nanoparticles. So, the AuNP-decorated aegle marmelos *(AM)* leaf has been demonstrated as a sensitive and low-cost

SERS platform for detection and analysis of Raman active samples. The usability of the proposed sensing platform has been demonstrated through detection of two antibiotics- Ceftriaxone (CEFTR) and Ceftiofur Sodium (CEF-Na) in cow milk samples. With the proposed SERS substrate, the targeted analyte with concentration as low as 0.1 ppm could be detected with a reasonably high reproducibility. Besides, ML-based classification model has been implemented in the present study to classify the antibiotics used in cow milk samples.

3. The fabrication of SERS substrates has also been performed by the electrochemical deposition (ED) of bimetallic NPs over the ITO-glass platform. Contrary to the direct deposition of NPs on a nanostructured surface, the ED provides good control over the morphological characteristics of the deposited NPs thereby provides more tuneability in the substrate fabrication process. Again, the presence of bimetallic NPs supports synergistic effect which further enhances scattered Raman signals enabling the trace quantification of analyte samples. With the optimized deposition cycles the size of the NPs can be tuned to generate a highly enhanced coupled LSPR field in the hotspot regions of the SERS platform; thereby enabling the trace detection of analyte molecules. The fabricated Cu-Au-ITO platform has been demonstrated for trace-detection of two antibiotics sulfamethoxazole (SFZ) and tetracycline hydrochloride (TCH) in egg samples. In the final step of this work ML classification model was integrated to identify the target specimens in real mixed samples.

4. In the next work, the functioning of electrospun PVA nanofiber as a SERS substrate has been explored. Following the ex-situ synthesis protocol, the AuNP-treated PVA nanofibers have been fabricated by the electrospinning technique. With the optimized voltage and rotor configuration, a sensitive SERS platform could be fabricated with good reproducibility and sensitivity characteristics. The optimized values of voltage and rotor speed of the ES setup provides relatively good control over the surface morphological properties of the nanofibers such as length and width of the fibers. The morphological property of the nanofiber are important as they affect the generation of EM hotspots which is crucial for the SERS based sensing schemes. The reliability of the proposed SERS platform has been demonstrated through the trace detection and quantification of enrofloxacin (ENX) and doxycycline hydrochloride (DCH) in chicken meat samples. Also, the multivariate dimensionality reduction technique PCA has been incorporated with the sensing scheme for segregation of the characteristic Raman signatures of the analyte in real meat samples.

5. In the final work, PVA nanofibers have been fabricated by ES and followed by O_2 plasma treatment for the generation of NPs. The major issue associ-

ated with the ex-situ synthesis process of nanofiber fabrication is the uneven distribution of nanoparticles, which sometimes may causes clustering and aggregation affecting the overall performance. The uneven distribution of AuNPs produces large variations in the intensities of the Raman signal. To compensate this issue, plasma treatment can be used instead of direct mixing of the NPs. The Plasma treatment facilitates a more uniform and controlled distribution of nanoparticles on the nanofiber surface, ensuring a homogenous structure which will eventually lead to the relatively uniform scattered Raman signal intensities. In this work, with the developed SERS substrate two antimicrobials fluconazole (FLU) and lincomycin (LIN) have been detected in trace concentrations. Further, for the real applicability of the designed platform, deep learning classification algorithm ANN has been implemented for rapid identification of the analytes in mixed samples.

References

[1] Trombini, C., Kazakova, J., Montilla-López, A., Fernández-Cisnal, R., Hampel, M., Fernández-Torres, R., Bello-López, M. Á., Abril, N., and Blasco, J. Assessment of pharmaceutical mixture (ibuprofen, ciprofloxacin and flumequine) effects to the crayfish Procambarus clarkii: A multilevel analysis (biochemical, transcriptional and proteomic approaches). *Environmental Research*, 200: 111396, 2021.

[2] Sreekanth, K., Vishal, G. N., Raghunandan, H. V., and Nitin, K. U. A review on managing of pharmaceutical waste in industry. *International Journal of PharmTech Research*, 6(3):899–907, 2014.

[3] Parashar, U. D., Alexander, J. P., Glass, R. I., on Immunization Practices, A. C., for Disease Control, C., (CDC), P., et al. Prevention of rotavirus gastroenteritis among infants and children. *Recommendations of the Advisory Committee on Immunization Practices (ACIP) MMWR Recomm Rep*, 55:1–13, 2006.

[4] Castanon, J. History of the use of antibiotic as growth promoters in European poultry feeds. *Poultry science*, 86(11):2466–2471, 2007. Number: 11 Publisher: Elsevier.

[5] Mulchandani, R., Wang, Y., Gilbert, M., and Van Boeckel, T. P. Global trends in antimicrobial use in food-producing animals: 2020 to 2030. *PLOS Global Public Health*, 3(2):e0001305, 2023. Publisher: Public Library of Science San Francisco, CA USA.

[6] Agyare, C., Boamah, V. E., Zumbi, C. N., and Osei, F. B. Antibiotic use in poultry production and its effects on bacterial resistance. *Antimicrobial resistanceA global threat*, pages 33–51, 2018. Publisher: IntechOpen London, UK.

[7] Hernández, F., Sancho, J. V., Ibáñez, M., and Guerrero, C. Antibiotic residue determination in environmental waters by LC-MS. *TrAC Trends in Analytical Chemistry*, 26(6):466–485, 2007. Publisher: Elsevier.

[8] Holstege, D. M., Puschner, B., Whitehead, G., and Galey, F. D. Screening and mass spectral confirmation of β-lactam antibiotic residues in milk using LC-MS/MS. *Journal of agricultural and food chemistry*, 50(2):406–411, 2002.

[9] Moreno-Bondi, M. C., Marazuela, M. D., Herranz, S., and Rodriguez, E. An overview of sample preparation procedures for LC-MS multiclass antibiotic determination in environmental and food samples. *Analytical and bioanalytical chemistry*, 395:921–946, 2009.

[10] Rehm, S. and Rentsch, K. M. LC-MS/MS method for nine different antibiotics. *Clinica Chimica Acta*, 511:360–367, Dec. 2020. ISSN 0009-8981. doi: 10.1016/j.cca.2020.11.001. URL https://www.sciencedirect.com/science/article/pii/S0009898120305209.

[11] Zhang, Y., Li, X. Q., Li, H. M., Zhang, Q. H., Gao, Y., and Li, X. J. Antibiotic residues in honey: A review on analytical methods by liquid chromatography tandem mass spectrometry. *TrAC Trends in Analytical Chemistry*, 110:344–356, 2019.

[12] Bargańska, Ż., Namieśnik, J., and Ślebioda, M. Determination of antibiotic residues in honey. *TrAC Trends in Analytical Chemistry*, 30(7):1035–1041, 2011.

[13] Drabińska, N., Hewett, K., White, P., Avison, M. B., Persad, R., Ratcliffe, N. M., and de Lacy Costello, B. Application of a solid-phase microextraction-gas chromatography-mass spectrometry/metal oxide sensor system for detection of antibiotic susceptibility in urinary tract infection-causing Escherichia coli–a proof of principle study. *Advances in Medical Sciences*, 67(1):1–9, 2022.

[14] Beale, D. J., Pinu, F. R., Kouremenos, K. A., Poojary, M. M., Narayana, V. K., Boughton, B. A., Kanojia, K., Dayalan, S., Jones, O. A. H., and Dias, D. A. Review of recent developments in GC–MS approaches to metabolomics-based research. *Metabolomics*, 14:1–31, 2018.

[15] Tsikas, D. Application of gas chromatography–mass spectrometry and gas chromatography–tandem mass spectrometry to assess in vivo synthesis of prostaglandins, thromboxane, leukotrienes, isoprostanes and related compounds in humans. *Journal of Chromatography B: Biomedical Sciences and Applications*, 717(1-2):201–245, 1998.

[16] Joshi, S. HPLC separation of antibiotics present in formulated and unformulated samples. *Journal of Pharmaceutical and Biomedical Analysis*, 28(5): 795–809, 2002.

[17] Charoenraks, T., Chuanuwatanakul, S., Honda, K., Yamaguchi, Y., and Chailapakul, O. Analysis of tetracycline antibiotics using HPLC with pulsed amperometric detection. *Analytical Sciences*, 21(3):241–245, 2005.

[18] McWhinney, B. C., Wallis, S. C., Hillister, T., Roberts, J. A., Lipman, J., and Ungerer, J. P. J. Analysis of 12 beta-lactam antibiotics in human plasma by HPLC with ultraviolet detection. *Journal of Chromatography B*, 878(22): 2039–2043, 2010.

[19] Doyuk, F. and Dost, K. Simultaneous determination of six antibiotics belonging to four different classes in chicken meat BY HPLC/DAD and verification BY LC-MS/MS. *Food Chemistry*, 426:136549, 2023.

[20] Swartz, M. HPLC detectors: a brief review. *Journal of Liquid Chromatography & Related Technologies*, 33(9-12):1130–1150, 2010.

[21] Horvai, G. and Pungor, E. Electrochemical detectors in HPLC and ion chromatography. *Critical Reviews in Analytical Chemistry*, 21(1):1–28, 1989.

[22] Singh, R. CV Raman and the Discovery of the Raman Effect. *Physics in Perspective*, 4:399–420, 2002.

[23] Raman, C. V. and Krishnan, K. S. A new type of secondary radiation. *Nature*, 121(3048):501–502, 1928.

[24] Raman, C. V. and Krishnan, K. S. The optical analogue of the Compton effect. *Nature*, 121(3053):711–711, 1928.

[25] Raman, C. V. A change of wave-length in light scattering. *Nature*, 121(3051): 619–619, 1928.

[26] Rostron, P., Gaber, S., and Gaber, D. Raman spectroscopy, review. *laser*, 21: 24, 2016.

[27] Lyon, L. A., Keating, C. D., Fox, A. P., Baker, B. E., He, L., Nicewarner, S. R., Mulvaney, S. P., and Natan, M. J. Raman spectroscopy. *Analytical Chemistry*, 70(12):341–362, 1998.

[28] Das, R. S. and Agrawal, Y. K. Raman spectroscopy: Recent advancements, techniques and applications. *Vibrational spectroscopy*, 57(2):163–176, 2011.

[29] Bruno, G. Classical theory of rayleigh and raman scattering. *The Raman Effect: A Unified Treatment of the Theory of Raman Scattering by Molecules*, pages 31–48, 2002.

[30] Hahn, D. W. Raman scattering theory. *Department of Mechanical and Aerospace Engineering, University of Florida*, 2007.

[31] Smith, E. and Dent, G. *Modern Raman spectroscopy: a practical approach*. John Wiley & Sons, 2019.

[32] Tannor, D. J. and Heller, E. J. Polyatomic Raman scattering for general harmonic potentials. *The Journal of Chemical Physics*, 77(1):202–218, 1982.

[33] Hecht, L. and Barron, L. D. Linear polarization Raman optical activity. The importance of the non-resonant term in the KramersHeisenbergDirac dispersion formula under resonance conditions. *Chemical physics letters*, 225(4-6):519–524, 1994.

[34] Ling, S., Imre, D. G., and Heller, E. J. Effects of the transition dipole in Raman scattering. *The Journal of Physical Chemistry*, 93(20):7107–7119, 1989.

[35] Dubessy, J., Caumon, M.-C., Rull, F., and Sharma, S. Instrumentation in Raman spectroscopy: elementary theory and practice. 2012.

[36] Cullum, B. M., Mobley, J., Chi, Z., Stokes, D. L., Miller, G. H., and Vo-Dinh, T. Development of a compact, handheld Raman instrument with no moving parts for use in field analysis. *Review of Scientific Instruments*, 71(4):1602–1607, 2000.

[37] Davis, K. L., Tedesco, J. M., and Shaver, J. M. Advances in fiber optic Raman instrumentation. In *Biomedical Applications of Raman Spectroscopy*, volume 3608, pages 148–156. SPIE, 1999.

[38] Turrell, G. The raman effect. In *Raman microscopy*, pages 1–25. Elsevier, 1996.

[39] Hudspeth, E. D., Cleveland, D., Batchler, K. L., Nguyen, P. A., Feaser, T. L., Quattrochi, L. E., Morenz, J., Balram, S. A., Michel, R. G., Zhou, J. X., et al. Teaching Raman spectroscopy in both the undergraduate classroom and

the laboratory with a portable Raman instrument. *Spectroscopy letters*, 39(1): 99–115, 2006.

[40] Sharma, B., Frontiera, R. R., Henry, A.-I., Ringe, E., and Van Duyne, R. P. SERS: Materials, applications, and the future. *Materials today*, 15(1-2):16–25, 2012. Publisher: Elsevier.

[41] Cialla, D., März, A., Böhme, R., Theil, F., Weber, K., Schmitt, M., and Popp, J. Surface-enhanced Raman spectroscopy (SERS): progress and trends. *Analytical and bioanalytical chemistry*, 403:27–54, 2012.

[42] Kneipp, J., Kneipp, H., and Kneipp, K. SERSa single-molecule and nanoscale tool for bioanalytics. *Chemical Society Reviews*, 37(5):1052–1060, 2008.

[43] Jiang, L., Hassan, M. M., Ali, S., Li, H., Sheng, R., and Chen, Q. Evolving trends in SERS-based techniques for food quality and safety: A review. *Trends in Food Science & Technology*, 112:225–240, 2021. URL https://www.sciencedirect.com/science/article/pii/S0924224421002582. Publisher: Elsevier.

[44] Fleischmann, M., Hendra, P. J., and McQuillan, A. J. Raman spectra of pyridine adsorbed at a silver electrode. *Chemical physics letters*, 26(2):163–166, 1974. Number: 2 Publisher: Elsevier.

[45] Jeanmaire, D. L. and Van Duyne, R. P. Surface Raman spectroelectrochemistry: Part I. Heterocyclic, aromatic, and aliphatic amines adsorbed on the anodized silver electrode. *Journal of electroanalytical chemistry and interfacial electrochemistry*, 84(1):1–20, 1977. Number: 1 Publisher: Elsevier.

[46] Albrecht, M. G. and Creighton, J. A. Anomalously intense Raman spectra of pyridine at a silver electrode. *Journal of the american chemical society*, 99(15): 5215–5217, 1977. Number: 15 Publisher: ACS Publications.

[47] Moskovits, M. Surface roughness and the enhanced intensity of raman scattering by molecules adsorbed on metals. *The Journal of Chemical Physics*, 69(9): 4159–4161, 1978.

[48] Pettinger, B., Wenning, U., and Wetzel, H. Surface plasmon enhanced raman scattering frequency and angular resonance of raman scattered light from pyridine on au, ag and cu electrodes. *Surface Science*, 101(1-3):409–416, 1980.

[49] Rubim, J. C., Corio, P., Ribeiro, M. C., and Matz, M. Contribution of resonance raman scattering to the surface-enhanced raman effect on electrode surfaces.

a description using the time dependent formalism. *The Journal of Physical Chemistry*, 99(43):15765–15774, 1995.

[50] Campion, A. and Kambhampati, P. Surface-enhanced Raman scattering. *Chem. Soc. Rev.*, 27:241–250, 1998. doi: 10.1039/A827241Z. URL http://dx.doi.org/10.1039/A827241Z.

[51] Campion, A., Ivanecky III, J. E., Child, C. M., and Foster, M. On the mechanism of chemical enhancement in surface-enhanced Raman scattering. *Journal of the American Chemical Society*, 117(47):11807–11808, 1995.

[52] Le Ru, E. and Etchegoin, P. *Principles of Surface-Enhanced Raman Spectroscopy: and related plasmonic effects*. Elsevier, 2008.

[53] Otto, A., Mrozek, I., Grabhorn, H., and Akemann, W. Surface-enhanced Raman scattering. *Journal of Physics: Condensed Matter*, 4(5):1143, feb 1992. doi: 10.1088/0953-8984/4/5/001. URL https://dx.doi.org/10.1088/0953-8984/4/5/001.

[54] Kim, J., Jang, Y., Kim, N.-J., Kim, H., Yi, G.-C., Shin, Y., Kim, M. H., and Yoon, S. Study of chemical enhancement mechanism in non-plasmonic surface enhanced Raman spectroscopy (SERS). *Frontiers in chemistry*, 7:582, 2019.

[55] Morton, S. M. and Jensen, L. Understanding the molecule- surface chemical coupling in SERS. *Journal of the American Chemical Society*, 131(11):4090–4098, 2009.

[56] Procházka, M. Surface-enhanced Raman spectroscopy. *Biological and medical physics, biomedical engineering*, pages 1–221, 2016.

[57] Fan, M., Andrade, G. F., and Brolo, A. G. A review on the fabrication of substrates for surface enhanced Raman spectroscopy and their applications in analytical chemistry. *Analytica chimica acta*, 693(1-2):7–25, 2011. Number: 1-2 Publisher: Elsevier.

[58] Adomaviit, S., Velika, M., and ablinskas, V. Detection of aspirin traces in blood by means of surface-enhanced Raman scattering spectroscopy. *Journal of Raman Spectroscopy*, 51(6):919–931, 2020. Publisher: Wiley Online Library.

[59] Choi, S., Jeong, H., Choi, K.-h., Song, J. Y., and Kim, J. Electrodeposition of Triangular Pd Rod Nanostructures and Their Electrocatalytic and SERS Activities. *ACS Applied Materials & Interfaces*, 6(4):3002–3007, Feb. 2014. ISSN 1944-8244, 1944-8252. doi: 10.1021/am405601g. URL https://pubs.acs.org/doi/10.1021/am405601g.

[60] Elias, J., Gizowska, M., Brodard, P., Widmer, R., Dehazan, Y., Graule, T., Michler, J., and Philippe, L. Electrodeposition of gold thin films with controlled morphologies and their applications in electrocatalysis and SERS. *Nanotechnology*, 23(25):255705, 2012. URL https://iopscience.iop.org/article/10.1088/0957-4484/23/25/255705/meta. Publisher: IOP Publishing.

[61] Bian, J.-C., Chen, Z.-D., Li, Z., Yang, F., He, H.-Y., Wang, J., Tan, J. Z. Y., Zeng, J.-L., Peng, R.-Q., Zhang, X.-W., and others. Electrodeposition of hierarchical Ag nanostructures on ITO glass for reproducible and sensitive SERS application. *Applied Surface Science*, 258(17):6632–6636, 2012. Publisher: Elsevier.

[62] Huan, T. N., Kim, S., Van Tuong, P., and Chung, H. AuAg bimetallic nanodendrite synthesized via simultaneous co-electrodeposition and its application as a SERS substrate. *RSC Adv.*, 4(8):3929–3933, 2014. ISSN 2046-2069. doi: 10.1039/C3RA44916E. URL http://xlink.rsc.org/?DOI=C3RA44916E.

[63] Jeong, H. and Kim, J. Electrodeposition of Nanoflake Pd Structures: Structure-Dependent Wettability and SERS Activity. *ACS Applied Materials & Interfaces*, 7(13):7129–7135, Apr. 2015. ISSN 1944-8244, 1944-8252. doi: 10.1021/acsami.5b02113. URL https://pubs.acs.org/doi/10.1021/acsami.5b02113.

[64] Rivera-Rangel, R. D., Navarro-Segura, M. E., Arizmendi-Morquecho, A., and Sánchez-Domínguez, M. Electrodeposition of plasmonic bimetallic Ag-Cu nanodendrites and their application as surface-enhanced Raman spectroscopy (SERS) substrates. *Nanotechnology*, 31(46):465605, 2020. Publisher: IOP Publishing.

[65] Pan, X., Bai, L., Pan, C., Liu, Z., and Ramakrishna, S. Design, Fabrication and Applications of Electrospun Nanofiber-Based Surface-Enhanced Raman Spectroscopy Substrate. *Critical Reviews in Analytical Chemistry*, pages 1–20, 2021. Publisher: Taylor & Francis.

[66] Li, C., Huang, Y., Li, X., Zhang, Y., Chen, Q., Ye, Z., Alqarni, Z., Bell, S. E. J., and Xu, Y. Towards practical and sustainable SERS: a review of recent developments in the construction of multifunctional enhancing substrates. *Journal of Materials Chemistry C*, 9(35):11517–11552, 2021.

[67] Farling, C. G., Stackaruk, M. C., Pye, C. C., and Brosseau, C. L. Fabrication of high quality electrochemical SERS (EC-SERS) substrates using physical vapour deposition. *Physical Chemistry Chemical Physics*, 23(36):20065–20072, 2021.

[68] Khan, A., Kumar, R. R., Cong, J., Imran, M., Yang, D., and Yu, X. CVD graphene on textured silicon: an emerging technologically versatile heterostructure for energy and detection applications. *Advanced Materials Interfaces*, 9(1): 2100977, 2022.

[69] Fan, M., Andrade, G. F. S., and Brolo, A. G. A review on recent advances in the applications of surface-enhanced Raman scattering in analytical chemistry. *Analytica chimica acta*, 1097:1–29, 2020.

[70] Barcelo, S. J., Wu, W., Li, X., Li, Z., and Williams, R. S. Nanoimprint lithography of plasmonic platforms for SERS applications. *Applied Physics A*, 121: 443–449, 2015.

[71] Jeon, T. Y., Kim, D. J., Park, S.-G., Kim, S.-H., and Kim, D.-H. Nanostructured plasmonic substrates for use as SERS sensors. *Nano Convergence*, 3:1–20, 2016.

[72] Shiohara, A., Wang, Y., and Liz-Marzán, L. M. Recent approaches toward creation of hot spots for SERS detection. *Colloidal synthesis of plasmonic nanometals*, pages 563–622, 2020.

[73] Lavine, B. and Workman, J. Chemometrics. *Analytical chemistry*, 80(12): 4519–4531, 2008.

[74] Wold, S. Chemometrics; what do we mean with it, and what do we want from it? *Chemometrics and intelligent laboratory systems*, 30(1):109–115, 1995.

[75] Adams, M. J. *Chemometrics in analytical spectroscopy*, volume 8. Royal Society of Chemistry, 2004.

[76] Meza Ramirez, C. A., Greenop, M., Ashton, L., and Rehman, I. U. Applications of machine learning in spectroscopy. *Applied Spectroscopy Reviews*, 56(8-10): 733–763, 2021.

[77] Blake, N., Gaifulina, R., Griffin, L. D., Bell, I. M., and Thomas, G. M. H. Machine learning of Raman spectroscopy data for classifying cancers: a review of the recent literature. *Diagnostics*, 12(6):1491, 2022.

[78] Beeram, R., Vepa, K. R., and Soma, V. R. Recent trends in SERS-based plasmonic sensors for disease diagnostics, biomolecules detection, and machine learning techniques. *Biosensors*, 13(3):328, 2023.

[79] Zhou, H., Xu, L., Ren, Z., Zhu, J., and Lee, C. Machine learning-augmented surface-enhanced spectroscopy toward next-generation molecular diagnostics. *Nanoscale advances*, 5(3):538–570, 2023.

[80] Gautam, R., Vanga, S., Ariese, F., and Umapathy, S. Review of multidimensional data processing approaches for Raman and infrared spectroscopy. *EPJ Techniques and Instrumentation*, 2:1–38, 2015.

[81] Goodacre, R., Graham, D., and Faulds, K. Recent developments in quantitative SERS: Moving towards absolute quantification. *TrAC Trends in Analytical Chemistry*, 102:359–368, 2018.

[82] Zhang, Z. Introduction to machine learning: k-nearest neighbors. *Annals of translational medicine*, 4(11), 2016.

[83] Othman, N. H., Lee, K. Y., Radzol, A. R. M., Mansor, W., Wong, P. S., and Looi, I. PCA-KNN for Detection of NS1 from SERS Salivary Spectra. In *Intelligent Information and Database Systems: 10th Asian Conference, ACIIDS 2018, Dong Hoi City, Vietnam, March 19-21, 2018, Proceedings, Part II 10*, pages 335–346. Springer, 2018.

[84] Li, W., Chen, G., Chen, M., Shen, K., Wu, C., Shen, W., and Zhang, F. PCA-WRKNN-assisted label-free SERS serum analysis platform enabling non-invasive diagnosis of Alzheimers disease. *Spectrochimica Acta Part A: Molecular and Biomolecular Spectroscopy*, 302:123088, 2023.

[85] Kang, S., Kim, I., and Vikesland, P. J. Discriminatory detection of ssDNA by surface-enhanced Raman spectroscopy (SERS) and tree-based support vector machine (Tr-SVM). *Analytical Chemistry*, 93(27):9319–9328, 2021.

[86] Li, B., Wu, Y., Wang, Z., Xing, M., Xu, W., Zhu, Y., Du, P., Wang, X., and Yang, H. Non-invasive diagnosis of Crohn's disease based on SERS combined with PCA-SVM. *Analytical Methods*, 13(44):5264–5273, 2021.

[87] Li, S., Zhang, Y., Xu, J., Li, L., Zeng, Q., Lin, L., Guo, Z., Liu, Z., Xiong, H., and Liu, S. Noninvasive prostate cancer screening based on serum surface-enhanced Raman spectroscopy and support vector machine. *Applied Physics Letters*, 105(9), 2014.

[88] Patle, A. and Chouhan, D. S. SVM kernel functions for classification. In *2013 International conference on advances in technology and engineering (ICATE)*, pages 1–9. IEEE, 2013.

[89] Botta, R., Chindaudom, P., Eiamchai, P., Horprathum, M., Limwichean, S., Chananonnawathorn, C., Patthanasettakul, V., Kaewseekhao, B., Faksri, K., and Nuntawong, N. Tuberculosis determination using SERS and chemometric methods. *Tuberculosis*, 108:195–200, 2018.

[90] Banaei, N., Moshfegh, J., Mohseni-Kabir, A., Houghton, J. M., Sun, Y., and Kim, B. Machine learning algorithms enhance the specificity of cancer biomarker detection using SERS-based immunoassays in microfluidic chips. *RSC advances*, 9(4):1859–1868, 2019.

[91] Moisoiu, T., Iancu, S. D., Burghelea, D., Dragomir, M. P., Iacob, G., Stefancu, A., Cozan, R. G., Antal, O., Bálint, Z., Muntean, V., et al. SERS liquid biopsy profiling of serum for the diagnosis of kidney cancer. *Biomedicines*, 10(2):233, 2022.

[92] Hu, Q., Sellers, C., Kwon, J. S.-I., and Wu, H.-J. Integration of surface-enhanced Raman spectroscopy (SERS) and machine learning tools for coffee beverage classification. *Digital Chemical Engineering*, 3:100020, 2022.

[93] Webb, G. I., Keogh, E., and Miikkulainen, R. Naïve Bayes. *Encyclopedia of machine learning*, 15(1):713–714, 2010.

[94] Erzina, M., Trelin, A., Guselnikova, O., Dvorankova, B., Strnadova, K., Perminova, A., Ulbrich, P., Mares, D., Jerabek, V., Elashnikov, R., et al. Precise cancer detection via the combination of functionalized SERS surfaces and convolutional neural network with independent inputs. *Sensors and Actuators B: Chemical*, 308:127660, 2020.

[95] Othman, N. H., Khuan, L. Y., Radzol, A. R. M., and Mansor, W. Detection of ns1 from sers spectra of adulterated saliva using ANN. *Advanced Science Letters*, 24(2):1138–1142, 2018.

[96] Seifert, S., Merk, V., and Kneipp, J. Identification of aqueous pollen extracts using surface enhanced Raman scattering (SERS) and pattern recognition methods. *Journal of Biophotonics*, 9(1-2):181–189, 2016.

[97] Somogyi, Z. and Somogyi, Z. Performance evaluation of machine learning models. *The Application of Artificial Intelligence: Step-by-Step Guide from Beginner to Expert*, pages 87–112, 2021.

[98] Flach, P. Performance evaluation in machine learning: the good, the bad, the ugly, and the way forward. In *Proceedings of the AAAI conference on artificial intelligence*, volume 33, pages 9808–9814, 2019.

[99] Freeman, R. G., Grabar, K. C., Allison, K. J., Bright, R. M., Davis, J. A., Guthrie, A. P., Hommer, M. B., Jackson, M. A., Smith, P. C., Walter, D. G., et al. Self-assembled metal colloid monolayers: an approach to SERS substrates. *Science*, 267(5204):1629–1632, 1995.

[100] Maitani, M. M., Ohlberg, D. A. A., Li, Z., Allara, D. L., Stewart, D. R., and Williams, R. S. Study of SERS chemical enhancement factors using buffer layer assisted growth of metal nanoparticles on self-assembled monolayers. *Journal of the American Chemical Society*, 131(18):6310–6311, 2009.